# New Insights on the Voltage Dependence of the $K_{Ca}3.1$ Channel Block by Internal TBA

Umberto Banderali, Hélène Klein, Line Garneau, Manuel Simoes, Lucie Parent, and Rémy Sauvé

Département de Physiologie, Membrane Protein Study Group, Faculté de Médecine, Université de Montréal, Montréal, Québec H3C 3J7, Canada

ABSTRACT We present in this work a structural model of the open IKCa ($K_{Ca}3.1$) channel derived by homology modeling from the MthK channel structure, and used this model to compute the transmembrane potential profile along the channel pore. This analysis showed that the selectivity filter and the region extending from the channel inner cavity to the internal medium should respectively account for 81% and 16% of the transmembrane potential difference. We found however that the voltage dependence of the IKCa block by the quaternary ammonium ion TBA applied internally is compatible with an apparent electrical distance δ of 0.49 ± 0.02 ($n = 6$) for negative potentials. To reconcile this observation with the electrostatic potential profile predicted for the channel pore, we modeled the IKCa block by TBA assuming that the voltage dependence of the block is governed by both the difference in potential between the channel cavity and the internal medium, and the potential profile along the selectivity filter region through an effect on the filter ion occupancy states. The resulting model predicts that δ should be voltage dependent, being larger at negative than positive potentials. The model also indicates that raising the internal $K^+$ concentration should decrease the value of δ measured at negative potentials independently of the external $K^+$ concentration, whereas raising the external $K^+$ concentration should minimally affect δ for concentrations >50 mM. All these predictions are born out by our current experimental results. Finally, we found that the substitutions V275C and V275A increased the voltage sensitivity of the TBA block, suggesting that TBA could move further into the pore, thus leading to stronger interactions between TBA and the ions in the selectivity filter. Globally, these results support a model whereby the voltage dependence of the TBA block in IKCa is mainly governed by the voltage dependence of the ion occupancy states of the selectivity filter.

KEY WORDS: calcium-activated potassium channel • quaternary ammonium • single file diffusion • EBIO • modeling



## INTRODUCTION

$Ca^{2+}$-activated potassium channels ($K(Ca^{2+})$) are present in most mammalian cell types, where their primary role is to establish a link between the various $Ca^{2+}$-based second messenger systems and the electrical properties of the cells. Three main classes of $Ca^{2+}$-activated potassium channels have been to date identified on the basis of their permeation properties and pharmacology (Vergara et al., 1998). These include the charybdotoxin- and iberiotoxin-sensitive $K_{Ca}1.1$ channels of large conductance (150–220 pS); the intermediate conductance (20–50 pS) IKCa channels ($K_{Ca}3.1$) inhibited by clotrimazole (Rittenhouse et al., 1997) and TRAM34 (Wulff et al., 2001), and the apamine-sensitive and -insensitive SK channels of small conductance ($K_{Ca}2.1$, $K_{Ca}2.2$, $K_{Ca}2.3$) (Kohler et al., 1996). In contrast to $K_{Ca}1.1$, the SK and IKCa channel gating process is voltage insensitive, and the $Ca^{2+}$ sensitivity in both channels is conferred by the $Ca^{2+}$-binding protein, calmodulin, constitutively bound to the channel proximal COOH-terminal regions (Khanna et al., 1999).

An important contribution to our understanding of the IKCa channel molecular identity came from the cloning of the hKCa4, hIK1, and hSK4 channels (Ishii et al., 1997; Joiner et al., 1997; Logsdon et al., 1997; Vandorpe et al., 1998; Warth et al., 1999). The IKCa channel is a tetrameric protein with each subunit comprising 427 amino acids organized in six transmembrane segments TM1–TM6 with a pore motif between segments 5 and 6. The three-dimensional (3D) structure of IKCa, however, remains unresolved. Docking simulations and binding studies using charybdotoxin analogues have revealed that the IKCa external vestibule is structurally similar to the external pore region of

Address correspondence to Rémy Sauvé, Département de Physiologie, Membrane Protein Study Group, Université de Montréal, C.P. 6128, Succursale Centre-ville, Montréal, Québec H3C 3J7, Canada. Fax: (514) 343-7146. email: remy.sauve@umontreal.ca

*Abbreviations used in this paper:* EBIO, 1-ethyl-2-benzimidazolinone; MTS, methanethiosulfonate; MTSET, [2-(trimethylammonium) ethyl]methanethiosulfonate bromide; NMDG, *N*-methyl-D-glucamine; QA, quaternary ammonium; SCAM, substituted cysteine accessibility method; TBA, tetrabutylammonium.


J. Gen. Physiol. © The Rockefeller University Press • 0022-1295/2004/10/333/16 $8.00
Volume 124 October 2004 333–348
http://www.jgp.org/cgi/doi/10.1085/jgp.200409145

other charybdotoxin-sensitive channels, such as Kv1.2 and Kv1.6 (Rauer et al., 2000). Sequence and secondary structure alignments also suggest a structural similarity between the proximal COOH-terminal region of IKCa (residues 395–430) and the calmodulin-binding domain of rSK2 (unpublished data), the structure of which has been resolved by X-ray crystallography (Schumacher et al., 2001). More recently, work from our laboratory has led to the first molecular description of the open/closed IKCa pore region using an approach combining the substituted cysteine accessibility method (SCAM), computer-based homology modeling, and single channel recordings (Simoes et al., 2002). The proposed IKCa models showed the V275, T278, and V282 residues as lining the channel pore, with V275 and T278 contributing to the formation of a central inner cavity ~10 Å wide. Fig. 1 presents the structures we propose for the open and closed IKCa obtained by homology modeling using the KcsA (Doyle et al., 1998) and MthK (Jiang et al., 2002a) channels as templates. Estimation of the distance between the α-carbons of corresponding residues along TM6 for subunits facing diagonally indicates a drastic widening of the pore starting at residue T278 upon channel opening. An analysis of the open channel structure reveals in addition that the inner vestibule exceeds 18 Å in diameter, suggesting that it should be wide enough to create a quasi isopotential continuum between the channel central cavity and the internal medium.

In this work we used the quaternary ammonium (QA) ion tetrabutylammonium (TBA) to investigate some of the structural features of the IKCa conduction pathway and probe the transmembrane potential profile within the IKCa open pore structure. QA ions are considered good blockers of $K^+$ channels and have been extensively used to characterize channel inner architecture. One of the main features of the blocking properties of QA ions concerns the voltage dependence of the channel block. For instance, studies in which the QA ions TEA or TBA were applied internally showed that the electrical distances that account for the voltage sensitivity of the channel block ranged from 0.2 (*Shaker* and MaxiKCa) (Villarroel et al., 1988; Ding and Horn, 2002; Thompson and Begenisich, 2003a; Li and Aldrich, 2004) up to 0.9 (Kir1.1 and Kir2.1) (Spassova and Lu, 1998, 1999; Guo and Lu, 2001) depending on channel types. X-ray data for the TBA-closed KcsA complex support a binding site for TBA located in the central cavity (Zhou et al., 2001). Assuming an equivalent position for the binding site in the open channel, electrical distances from 0.2 to 0.9 could be indicative of pore structures where a significant fraction of the transmembrane potential drop occurs over the region extending from the channel central cavity to the internal medium. However, these values might be difficult to reconcile with an isopotential continuum between the channel central cavity and the internal medium, as suggested by the MthK channel structure. The blocking potency of internal QA ions also depends on the structural parameters controlling the accessibility of the ions to the interaction site. Notably, there are considerable variations in the entry rate of individual QA ions depending on channel types. For instance, the entry rate measured for TBA in zero current conditions was found to vary from 0.004 $\mu M^{-1}s^{-1}$ for the Kir1.1 and Kir2.1 inward rectifiers up to 0.55 $\mu M^{-1}s^{-1}$ for *Shaker* (Guo and Lu, 2001; Ding and Horn, 2002). These variations are likely to reflect gross differences in the channel inner vestibule geometry.

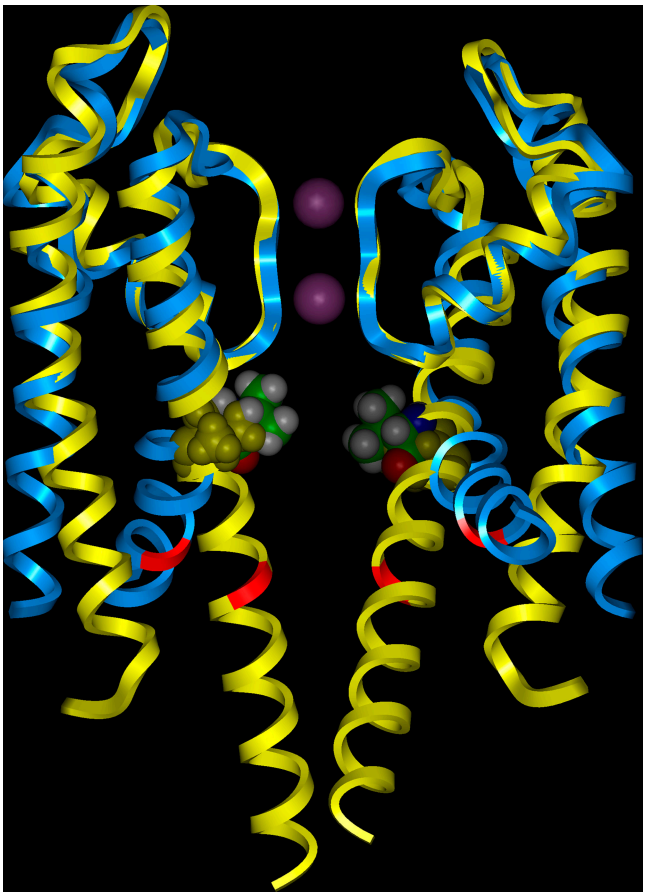

FIGURE 1. 3D representation of the proposed structure for the open (blue) and closed (yellow) IKCa channel. Only two of the four monomers are presented for clarity. The two structures were superimposed to illustrate the structural changes related to channel opening. The V275 residue, shown in a VDW representation, is colored in yellow for the closed channel and in atom color code for the open channel configuration. The location of the A283 residue is marked in red. According to these models, the V275 residue is lining the central cavity, whereas the A283 residue is located in the channel inner vestibule. The model also includes two ions in the selectivity filter. Models were constructed by homology modeling using the KcsA and MthK bacterial channels as templates (see MATERIALS AND METHODS for details). Graphical representation was generated using the InsightII software (Accelrys Inc.).

In this work, we measured the kinetics and the voltage dependence of the IKCa block by internal TBA. Our results confirm that the V275 residue is lining the channel central pore cavity and contributes to the architecture of the TBA interaction site. We also demonstrate that the voltage dependence of the IKCa block by TBA presents a complex pattern with an apparent electrical distance of 0.49 at negative potentials. Using the structure proposed for the open IKCa configuration and the recent model of Berneche and Roux (2003) describing the single file diffusion of $K^+$ in the KcsA selectivity filter, we show that the observed dependence of the TBA block reflects the ion occupancy state of the selectivity filter rather than the actual potential difference between the channel inner cavity and the internal medium.

## MATERIALS AND METHODS

### *Cloning, Sequencing and Site-directed Mutagenesis of the IKCa Channel*

IKCa channel cDNAs were obtained by RT-PCR from HeLa cells as described previously (Simoes et al., 2002). The resulting PCR product was identical to the sequences reported for the hKCa4 (GenBank/EMBL/DDBJ accession no. AF033021), hIK1 (AF022150), and hSK4 (AF000972) channels. Site-directed mutagenesis of IKCa channel was performed using the QuickChange Site-Directed Mutagenesis kit (Stratagene). Point mutations were obtained by using 25-mer mutated oligonucleotides with the wild-type IKCa as template. Mutations were confirmed by sequencing the entire coding region on both strands.

### *Oocytes*

Mature oocytes (stage V or VI) were obtained from *Xenopus laevis* frogs anesthetized with 3-aminobenzoic acid ethyl ester. The follicular layer was removed by incubating the oocytes in a $Ca^{2+}$-free Barth's solution containing collagenase (1.6 mg/ml; Sigma-Aldrich) for 45 min. The composition of the Barth's solution was (in mM) 88 NaCl, 3 KCl, 0.82 $MgSO_4$, 0.41 $CaCl_2$, 0.33 $Ca(NO_3)_2$, and 5 HEPES (pH 7.6). Defolliculated oocytes were stored at 18°C in Barth's solution supplemented with 5% horse serum, 2.5 mM Na-pyruvate, 100 U/ml penicillin, 0.1 mg/ml kanamycin, and 0.1 mg/ml streptomycin. Oocytes were patched 3–5 d after coinjection of 0.92–9.2 ng of the cDNA coding for IKCa in pMT21 and 1.38 ng of cDNA coding for a green fluorescent protein that was used as a marker for nuclear injection.

Prior to patch clamping, defolliculated oocytes were kept in a hyperosmotic solution containing (in mM) 250 KCl, 1 $MgSO_4$, 1 EGTA, 50 sucrose, and 10 HEPES buffered at pH 7.4 with KOH. The vitelline membrane was then peeled off using fine forceps, and the oocyte was transferred to a superfusion chamber for patch clamp measurements.

### *Solutions*

The bath and patch pipette solutions consisted of (in mM) 200 $K_2SO_4$, 1.8 $MgCl_2$, 0.025 $CaCl_2$, 25 HEPES, buffered at pH 7.4 with KOH. The use of sulfate salts prevented contributions from endogenous $Ca^{2+}$-dependent chloride channels while enabling to chelate contaminant divalent cations such as $Ba^{2+}$ (maximum free $Ba^{2+}$ concentration: 0.5 nM in 200 mM $K_2SO_4$). Calcium-free solutions were prepared by omitting $CaCl_2$ from the 200 mM $K_2SO_4$ solution and adding 1 mM EGTA. Solutions with different potassium concentrations were prepared using NMDG as replacing ion and titrated with $H_2SO_4$. Unless specified otherwise, potassium ion concentrations are expressed as potassium activities. Activity coefficients for the various $K_2SO_4$ solutions were obtained from literature (Robinson and Stokes, 1959). The potassium ion activity for each solution reads: 225 mM for the 400 mM $K_2SO_4$ solution; 140 mM for the 200 mM $K_2SO_4$ solution; 60 mM for the 50 mM $K_2SO_4$ solution; and 2 mM for the 1 mM $K_2SO_4$ solution. TBA was dissolved directly into the bath solution at the desired concentration. MTSET (Toronto Research Chemicals Inc.) was added into the recording saline directly before use. EBIO (Tocris Cookson Inc.) was first dissolved in DMSO and then diluted in the experimental solution.

### *Rapid Solution Changes*

Internal solution changes in inside-out recordings were performed using an RSC-160 rapid solution changer system (Bio-Logic). The bath solution could be fully exchanged within <30 ms as measured by the variation in patch pipette resistance when $BaCl_2$ (10 mM)-containing patch electrodes were exposed to a 200 mM KCl plus 200 μM $K_2SO_4$ bath solution. Typically, $Ca^{2+}$-free and TBA-containing bath solutions were perfused in successive 4-s periods, separated by 5-s washouts with the control solution.

### *Patch Clamp Recordings*

Single channel recordings were performed in the inside-out patch clamp configuration using a List EPC-7 amplifier (List Medical). Patch pipettes were pulled from borosilicate capillaries using a Narishige pipette puller (Model PP-83) and used uncoated. The resistance of the patch electrodes ranged from 4 to 6 mΩ. Data acquisition was performed using a TL-1 DMA interface (Axon Instruments) at a sampling rate of 1.0 kHz with filtering at 500 Hz. Experiments were performed at room temperature (22°C).

### *TBA Protection Experiments*

TBA protection experiments were performed by measuring the change in MTSET accessibility to cysteines engineered either at position 275 or 283 in the presence or absence of TBA in the internal solution. Basically, MTSET (5 mM) was applied for 1 s during single 2-s TBA application (5 mM). Each TBA application was followed by a 2-s washout period with the standard 200 $K_2SO_4$ solution (see Fig. 3). Control experiments performed without TBA were performed according to the same perfusion protocol.

### *Data Analysis*

Kinetics of intracellular TBA block were determined according to the following scheme:

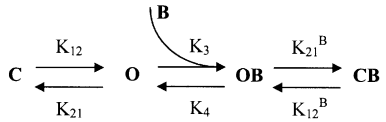

(SCHEME 1)

where B is the concentration of the blocking agent, $K_{12}$ and $K_{21}$ the rates of channel opening and closing, respectively, $K_{12}^B$ and $K_{21}^B$ the rates of channel opening and closing with the channel in the blocked configuration, $K_3$ the entry rate in $\mu M^{-1}s^{-1}$ of the blocking agent, and $K_4$ the dissociation rate of the blocker (for example see Holmgren et al., 1997). $K_{12}$ and $K_{21}$ represent in this case the rates of opening and closing seen by the blocking agent averaged over all the channel states leading to observable transitions (see appendix in Garneau et al., 2003). It is assumed in

Scheme 1 that the blocker cannot enter the channel when in the closed configuration. It follows from this scheme that the fraction of current block $f_B$ is given by

$$f_B = \frac{I_B}{I_{Max}} = \frac{1}{\left(1 + \frac{B}{IC_{50}}\right)}, \quad (1)$$

with $I_{Max}$ and $I_B$ the currents before and after application of the blocking agent and

$$IC_{50} = \frac{K_4\zeta}{K_3}, \quad (2)$$

where $\zeta = Po^B/Po$ with $Po = K_{12}/(K_{12} + K_{21})$ is the open probability of the channel before inhibition by the blocker (Ding and Horn, 2002), and $Po^B = K_{12}{}^B/(K_{12}{}^B + K_{21}{}^B)$ the probability that the channel will be in the open blocked configuration. If the binding of the blocker to the channel does not modify gating ($\zeta = 1$), it follows from Eq. 2 that $IC_{50}$ becomes independent of the channel open probability.

The blocker effective exit rate, $K_4Po\zeta$, can be obtained by measuring the rate at which the macroscopic current recovers after removal of the blocker. According to the Scheme 1, current recovery after removal of the blocker is given by

$$I(t) = I_{Max} + A1e^{-(K_{12}+K_{21})t} + A2e^{-\omega 1t} + A3e^{-\omega 2t}, \quad (3)$$

where A1, A2, and A3 are constants and ω1 and ω2 transitions rates such that

$$\omega 1 + \omega 2 = K_4 + K_{12}{}^B + K_{21}{}^B \quad (4)$$

$$\omega 1\omega 2 = K_4K_{12}{}^B. \quad (5)$$

In conditions where the dissociation rate is slow ($K_{12}{}^B + K_{21}{}^B >> K_4$), ω1 and ω2 can be approximated as

$$\omega 1 \cong K_{12}{}^B + K_{21}{}^B \quad (6)$$

and

$$\omega 2 \cong K_4\frac{K_{12}{}^B}{(K_{12}{}^B + K_{21}{}^B)}. \quad (7)$$

Assuming in addition that $K_{12} + K_{21} >> K_4$, Eq. 3 reduces to a single exponential with a time constant $\tau_{on}$ given by

$$\tau_{on} = \frac{1}{\omega 2} = \frac{1}{K_4Po\zeta}. \quad (8)$$

It follows from Eq. 2 that the effective entry rate of the blocker can now be obtained from

$$K_3Po = \frac{1}{\tau_{on}IC_{50}}. \quad (9)$$

In the present study, $I_B$ and $I_{Max}$ were estimated using the QuB package (Qin et al., 1996, 1997). The time constant $\tau_{on}$ was obtained from the time course of the current recovery after TBA removal fitted to a single exponential function using the Origin 6.1 software (Origin; Microcal Software Inc.). $IC_{50}$ values were computed by fitting the TBA dose–response inhibition curves to Eq. 1 using the logistic function in Origin 6.1. The analytic solution of the kinetic scheme presented in Fig. 6 A and model-based simulations were generated with the Mathematica 4.1 software (Wolfram Research Inc.).

In conditions where single channel events could be recorded, the single channel conductance was estimated from current amplitude histograms as described previously (Morier and Sauvé, 1994). For multichannel recordings, Po was determined from noise analysis by measuring the ratio

$$\frac{\sigma^2}{<I>} = (1 - Po)Io \quad (10)$$

as a function of the applied voltage V with $\sigma^2$ the steady-state current variance, <I> the current mean value, and Io the channel unitary current. Po was computed as

$$Po = 1 - \frac{\Lambda_{noise}}{\Lambda_{single\ channel}}, \quad (11)$$

where $\Lambda_{noise}$ is the conductance derived from the plot of $\sigma^2/<I>$ as a function of V and $\Lambda_{single\ channel}$ the unitary channel conductance.

### *Statistical Analysis*

Statistical significance was analyzed using unpaired Student's *t* test. $P < 0.01$ was considered statistically significant.

### *Homology Modeling*

Automated homology modeling was performed with Modeller V6.1 (Sali and Blundell, 1993) and involved the generation of 50 models of the IKCa channel pore using the MthK and KcsA channel structures as templates (Protein Data Bank entry 1LNQ). Energy minimization was carried on the model with the lowest objective function (roughly related to the energy of the model) using CHARMm.

### *Electrostatic Energy Profile*

The atomic structure of the IKCa model was inserted in a 25-Å-thick membrane represented as a continuum medium with a dielectric constant of 2. No electrolyte was included in the bulk solution and in the potassium channel central cavity, but a 17-Å diameter cylindrical aqueous pore with a dielectric constant of 80 was added along the pore axis (z). The electrostatic contribution to the free energy needed to transfer a $K^+$ from the bulk solution to a position z along the channel pore was calculated as

$$\Delta\Delta G_{elec,i(z)} = (\Delta G_{i(z)\text{-}c} - \Delta G_c - \Delta G_{i(z)}), \quad (12)$$

where $\Delta G_{i(z)\text{-}c}$ is the electrostatic energy of the channel with an ion at the position z with $x = y = 0$, $\Delta G_c$ is the electrostatic energy of the channel with no ion, and $\Delta G_{i(z)}$ the electrostatic energy of the $K^+$ ion in the bulk solution. The finite-difference calculations were performed using the PBEQ module of the biomolecular simulation program CHARMm (for example see Roux, 1997). The numerical calculations were performed using a standard relaxation algorithm (Warwicker and Watson, 1982). The complete system was mapped onto a cubic grid, and the Poisson equation solved numerically. The total electrostatic potential was calculated at each point of the grid by solving the finite difference Poisson equation. Calculations were performed in two steps, first using spacing of 1.0 Å (130 points, with periodic boundary conditions in the membrane plane), followed by more precise calculations around the main region with a grid spacing of 0.5 Å. A hydrogen minimization procedure was performed between each ion position.

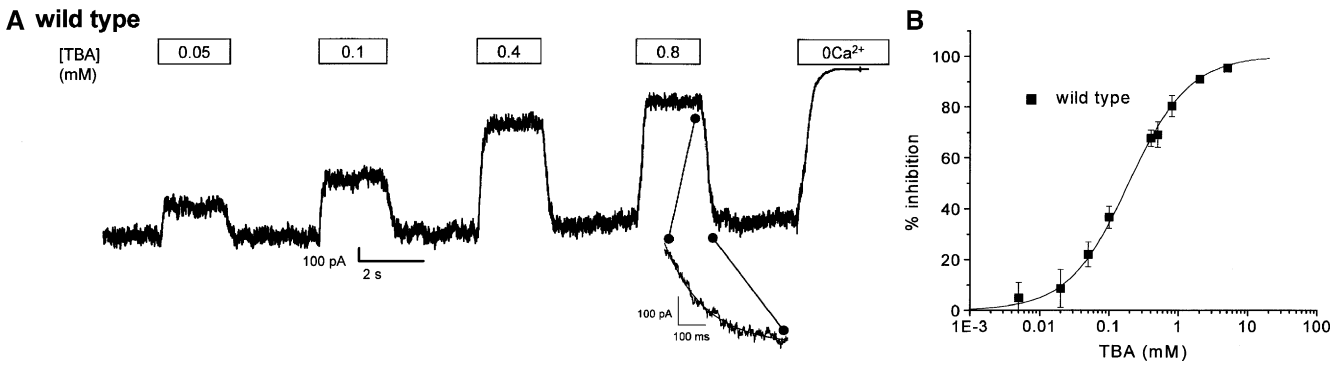


FIGURE 2. IKCa block by TBA. (A) Perfusion protocol used to measure TBA block dose–response curves. Inside-out current records were measured in symmetrical 200 mM $K_2SO_4$ + 100 μM EBIO conditions at a constant membrane potential of −60 mV. Increasing concentrations of internal TBA were applied for short periods (2 s) separated by 2 s of washout. The percentage of inhibition was calculated with 100% corresponding to the current level before each TBA application, and 0% the current recorded in zero $Ca^{2+}$ conditions. The magnification shows the exponential time course of the current recovery ($\tau_{on}$) after TBA removal. (B) Dose–response curve of IKCa block by TBA. The continuous line was computed from Eq. 1 with $IC_{50}$ = 192 μM.

## RESULTS

### *Block of IKCa Wild Type by TBA*

TBA has been documented to block the pore of a wide variety of $K^+$ channels by entering the open channel from the cytoplasmic side up to the channel inner cavity. Experiments were conducted to characterize the effects of TBA on wild-type IKCa channels expressed in *Xenopus laevis* oocytes. Fig. 2 A shows representative inside-out current traces in which TBA was applied internally at a constant membrane potential of −60 mV. As seen, application of TBA at concentrations ranging from 50 to 800 μM caused a dose-dependent inhibition of the IKCa current that was fully reversible after washout of the QA ion. In addition, the time course of the current recovery after TBA washout is shown to be accounted for by a single exponential (see Eqs. 3–8). The dose–response curve for current inhibition measured at −60 mV is presented in Fig. 2 B. Data points could be well fitted to Eq. 1 with $IC_{50}$ equal to 192 ± 7 μM ($n$ = 12), indicating a bimolecular reaction involving one inhibitor per ion channel as hypothesized in the kinetic Scheme 1.

### *TBA Access to the Channel Cavity*

Crystallization of the bacterial channel KcsA in the presence of TBA has provided direct evidence for TBA binding in the channel central cavity (Zhou et al., 2001). An analysis of the TBA binding site in the closed KcsA structure indicates that the external Van der Waals surface of TBA is in close contact with the T75 and I100 pore lining residues. The 3D model of the closed IKCa we derived through homology modeling using the KcsA channel as template suggests a structural equivalence between I100 in KcsA and V275 in IKCa (Simoes et al., 2002). This prediction was confirmed by SCAM experiments where the V275C mutant channel in the open state was strongly inhibited by the positively charged MTSET reagent applied internally (Simoes et al., 2002). Fig. 1 shows a superimposed representation of the proposed IKCa channel model structures in the closed and open configurations. The structure of the open channel was obtained by homology modeling with MthK as template (see MATERIALS AND METHODS). In the open configuration, the residue V275 is predicted to be lining the IKCa channel central cavity. In contrast, the A283 residue is expected to be located in the channel inner vestibule at the entrance of the cavity region. Notably, internal application of MTSET to the A283C mutant, resulted in an increase in channel activity, coupled to a partial inhibition of the single channel currents (Simoes et al., 2002).

To identify the TBA binding site in the IKCa channel, inside-out experiments were undertaken to evaluate the ability of TBA to protect cysteines engineered either at position 275 or 283 against a chemical modification by the MTSET reagent (see MATERIALS AND METHODS). An example of a TBA protection experiment with the V275C channel is presented in Fig. 3 A. As seen, 5 mM TBA completely and reversibly blocked the V275C currents. The change in MTSET accessibility due to the presence of TBA is summarized in Fig. 3 B. These results show an eightfold increase in the time constant for MTSET-induced inhibition from 18 ± 1 s ($n$ = 2) in the absence of TBA, to 147 ± 5 s ($n$ = 4) with TBA. This observation indicates that TBA had access to a site close enough to V275 as to interfere with the accessibility of MTSET to the cysteine at position 275, in agreement with the structural data of the KcsA + TBA complex (Zhou et al., 2001). In contrast, the results in Fig. 3 C show that TBA failed to affect the time course of the stimulatory action of MTSET on the A283C channel, indicating that the TBA binding site is located closer to the cavity region than to the inner vestibule.

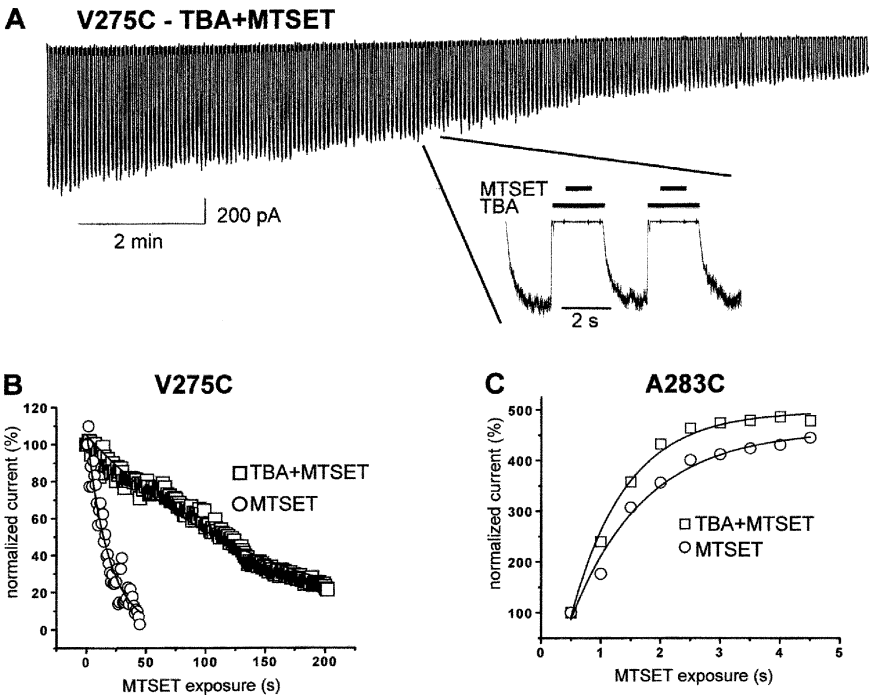


FIGURE 3. TBA prevents V275C mutant from reacting with MTSET. (A) Perfusion protocol used to test the effectiveness of TBA to protect Cys residues engineered either at position 275 or 283 from being covalently modified by MTSET. Inside-out current records measured in symmetrical 200 mM $K_2SO_4$ + 100 μM EBIO conditions at a constant membrane potential of −60 mV. The perfusion protocol consisted in applying MTSET (5 mM) for 1 s during each 2-s internal application of TBA at 5 mM. Recovery from channel block was measured within the 2-s washout periods separating successive TBA applications. As a result, MTSET was applied for 1 s for each perfusion cycle of 4 s. (B) In the absence of TBA, internal applications of MTSET resulted in a gradual decrease of the V275C currents with a time constant of 18.6 ± 0.9 s (circles; $n = 2$). The inhibitory effect of MTSET was considerably impaired in the presence of internal TBA (5 mM) with a time constant of inhibition estimated at 147 ± 2 s (squares; $n = 4$). These results indicate that the TBA interaction site should be located close enough to the cavity lining 275C residue as to reduce its accessibility to MTSET. (C) Similar site protection experiments were performed with the A283C mutant. Internal application of MTSET (5 mM) caused in this case a large increase of the A283C-induced currents. The current activation recorded either with (squares) or without (circles) internal TBA showed no significant differences in time constant, with values of 1.23 ± 0.18 s ($n = 2$) and 0.92 ± 0.08 s ($n = 2$), respectively. These results argue for a TBA binding site located in close proximity of the cavity lining V275 residue, distant from A283.

*TBA Block and IKCa Channel Open Probability*

The analytical expression presented in Eq. 2 predicts that the concentration for half inhibition, $IC_{50}$, should depend on the parameter $\zeta = Po^B/Po$, which accounts for the change in open probability due to the presence of TBA in the channel cavity (see MATERIALS AND METHODS). As a result, $IC_{50}$ measurements should be independent of the channel open probability, provided the channel gating behavior is not affected by the binding of TBA to its site ($\zeta = 1$). This hypothesis was tested by modifying the channel open probability using the IKCa opener EBIO. An example of inside-out recording illustrating the effects of EBIO applied internally is presented in Fig. 4 A. As seen, the addition of internal EBIO led to a substantial increase in the current mean value and variance. Noise analysis performed on the recordings before and after the addition of 100 μM EBIO to the internal medium revealed an increase in the channel open probability Po from 0.17 ± 0.08 ($n = 6$) to 0.50 ± 0.09 ($n = 6$) (see Eq. 11 and Fig. 4 D). The effect of EBIO (100 μM) on the dose response curve of the IKCa block by TBA is illustrated in Fig. 4 B. Our results show a significant decrease of the $IC_{50}$ value from 298 ± 20 μM ($n = 11$) in the absence of EBIO to 192 ± 7 μM ($n = 12$) in EBIO conditions ($P < 0.0001$). These results indicate that the presence of TBA in the channel cavity affects gating.

*Voltage Dependence of the TBA Block*

Fig. 5 A summarizes the effect of voltage on the TBA dose–response curve for voltages ranging from −30 to −120 mV, measured in EBIO conditions. As seen, negative membrane voltages resulted in a rightward shift of the TBA dose–response curve. The variation in $IC_{50}$ as a function of voltage is presented in Fig. 5 B. Clearly, the voltage dependence of the TBA block shows a complex behavior with a stronger voltage dependence at negative than at positive potentials. In the former case, the data could be approximated to a single exponential function of the form $IC_{50} = IC_{50}(0)\ \exp(-\delta Vq/KT)$, where δ is the fraction of the transmembrane potential through which internal TBA moves to reach its site (Woodhull, 1973), V the applied voltage, q, K, and T the electrical charge, the Boltzmann constant, and the temperature, respectively. Estimations of the electrical distance δ within the voltage range −120 to −30 mV led to a value of 0.49 ± 0.02 ($n = 6$).

*Channel Gating and TBA Block*

According to Scheme 1, it is hypothesized that TBA can be trapped inside the channel cavity upon closing. The effect of changing the channel open probability on the voltage dependence of the TBA entry and exit rates was thus investigated using EBIO as stimulating

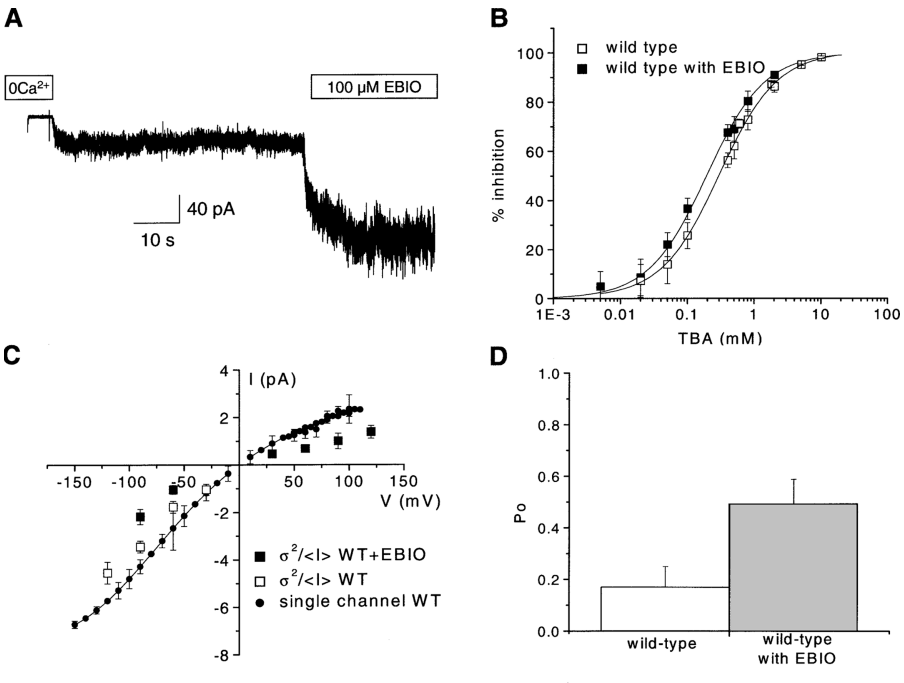


FIGURE 4. Effect of EBIO on the IKCa channel open probability and TBA sensitivity. (A) Inside-out recording of IKCa channel showing the effect of the internal addition of 100 µM EBIO. Experiments performed in symmetrical 200 mM $K_2SO_4$ + 25 µM internal $Ca^{2+}$ conditions at a constant membrane potential of −60 mV. As seen, EBIO elicited a clear increase in the current mean value and variance. EBIO did not modify, however, the single channel current amplitude (not depicted). (B) TBA block dose–response curves with (filled squares) and without (open squares) 100 µM EBIO added to the internal solution. The addition of EBIO decreased the apparent $IC_{50}$ value from 298 ± 20 µM ($n$ = 11) to 192 ± 7 µM ($n$ = 12) ($P < 0.0001$). (C) Variation of the ratio $\sigma^2/<I>$ (Eq. 10) as a function of voltage for the wild-type IKCa channel with (filled squares) and without EBIO (open squares). The channel open probability was computed according to Eq. 11 using as reference the IKCa channel I/V curve obtained from single channel recordings (dots). The continuous line represents the prediction of the model in Fig. 6 A with: $k1(0) = 0.75 \times 10^9\ s^{-1}$, $k2(0) = 2.5 \times 10^9\ s^{-1}$, $k1_B(0) = k3(0) = 0.165 \times 10^9\ s^{-1}$, $k2_B(0) = k4(0) = 11.5 \times 10^9\ s^{-1}$, $ki(0) = 1.8 \times 10^{10}\ M^{-1}s^{-1}$, $ke(0) = 1.26 \times 10^9\ s^{-1}$, $ko(0) = 6.5 \times 10^8\ M^{-1}s^{-1}$, $kx(0) = 3.0 \times 10^7\ s^{-1}$, $k5(0) = 1.25 \times 10^9\ s^{-1}$, $k6(0) = 2.7 \times 10^9\ s^{-1}$, $\alpha = \beta = 0.84$, $f = 0.22$. (D) Effect of EBIO on the IKCa open probability Po as measured by noise analysis according to Eq. 11. EBIO increased Po from 0.17 ± 0.08 ($n$ = 6) to 0.50 ± 0.09 ($n$ = 6).

agent. As seen in Fig. 5 (C and D), stimulation by EBIO increased the effective entry (PoK3) and exit (Po ζ K4) rates 3.8-fold and 2.7-fold, respectively, over the whole voltage range with no significant change in the voltage dependence of the TBA block. The observation that the TBA exit rate depends on the channel open probability supports the linear kinetic scheme proposed in Scheme 1 and suggests that TBA can be trapped in the cavity upon channel closing. This proposal is also supported by the results presented in Fig. 5 D, where the unbiased entry rates K3 (diamonds) could be estimated from the effective entry rates PoK3 measured either in the absence or presence of EBIO, using Po values equal to 0.13 and 0.49 in control and EBIO conditions, respectively. The latter values are well within the Po range estimated by noise analysis (Fig. 4 D). Finally, the data in Fig. 5 C show that the TBA exit rate decreased an e-fold factor per 85 mV over the voltage range −120 to 0 mV for an electrical distance $\delta = 0.29$. In contrast, the effective entry rate Po K3 increased with an e-fold factor per 150 mV over the same voltage range for a δ value corresponding to 0.16. Interestingly, the apparent electrical distances δ obtained for the kinetic parameters of TBA block ($\delta entry + \delta exit = 0.45$) are in good agreement with the equilibrium $\delta = 0.49$ obtained from the changes in $IC_{50}$ as a function of voltage.

*Modeling of the Voltage Dependence of the TBA Block*

According to electrostatic potential calculations based on the MthK crystal structure, the channel cavity and the cytoplasmic medium should form a continuous isopotential region (Jiang et al., 2002b). This property reflects in essence the broad opening of the vestibule predicted by the MthK structure (Fig. 1). Fig. 6 B presents the membrane potential profile obtained by solving the Poisson-Boltzmann equation for the TM5-pore-TM6 region derived by homology modeling for the wild-type IKCa (Fig. 1). These calculations indicate that the potential difference between the cavity ($z = 0$) and the cytoplasmic medium accounts for <16% of the potential applied across the membrane with 81% of the voltage drop restricted to the selectivity filter. In turn, the difference in potential between adjacent sites within the selectivity filter ([S2-S1], [S3-S2], [S4-S3]) should represent 23% of the membrane potential compared with 12% between the S0 and S1 binding sites and 3% between the cavity (S5) and the S4 site. Finally, there should be no difference in potential between the external binding site S0 and the external solution. On the basis of the proposed model for the open IKCa channel, it is clear that a simple model whereby the voltage dependence of the TBA block arises from the difference in potential between the in-

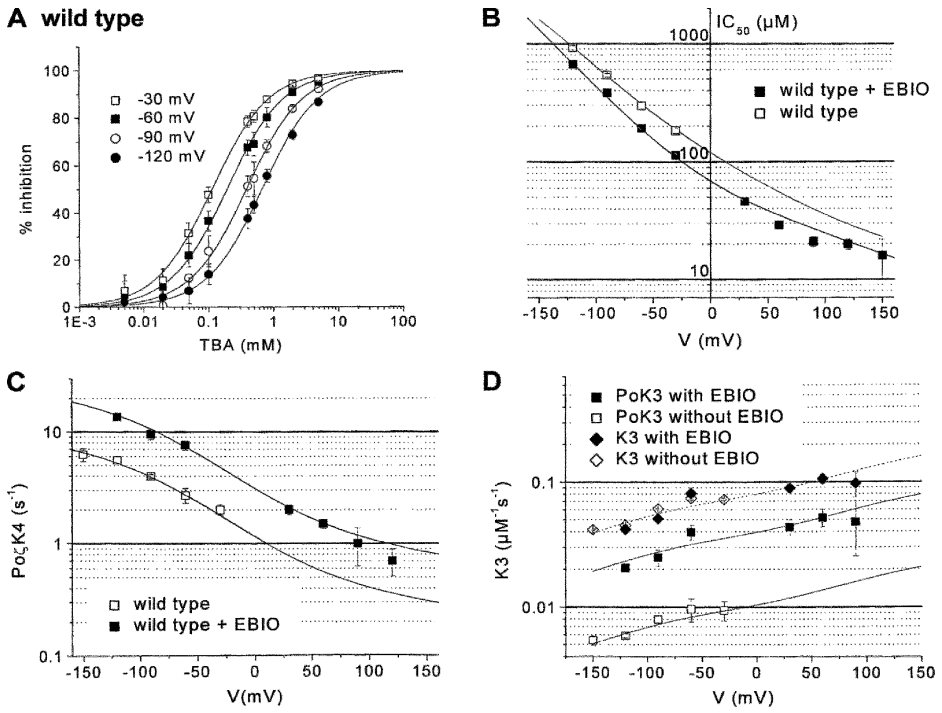


FIGURE 5. Voltage dependence of the TBA-induced IKCa channel block. (A) Dose–response curves of IKCa block by TBA measured in EBIO (100 μM) conditions at membrane potentials ranging from −120 to −30 mV. The concentration for half inhibition $IC_{50}$ was computed by fitting the experimental data to Eq. 1. Increasing hyperpolarizing voltages rightward shifted the dose–response curves with $IC_{50}$ values of 666 ± 17 μM ($n$ = 6) and 113 ± 4 μM ($n$ = 6) at −120 and −30 mV, respectively. (B) Plot of $IC_{50}$ as a function of voltage measured in the presence (filled squares) and in the absence (open squares) of EBIO. Data points within the voltage range −120 to −30 mV were fitted to a single exponential function resulting in an electrical distance of 0.49 ± 0.02 ($n$ = 6). The continuous lines were computed from the model presented in Fig. 6 A using Eqs. 13 and 14 with $IC_{50} = \langle K_B4\rangle/\langle K_B3\rangle$. The best fit was obtained with $K_B41(0) = 8\ s^{-1}$, $K_B42(0) = 28\ s^{-1}$, $K_B43(0) = 1.7\ s^{-1}$, $K_B31(0) = 0.022\ s^{-1}\mu M^{-1}$, $K_B32(0) = 0.07\ s^{-1}\mu M^{-1}$, $K_B33(0) = 0.1\ s^{-1}\mu M^{-1}$ with EBIO and $K_B41(0) = 2.9\ s^{-1}$, $K_B42(0) = 10.4\ s^{-1}$, $K_B43(0) = 0.63\ s^{-1}$, $K_B31(0) = 0.006\ s^{-1}\mu M^{-1}$, $K_B32(0) = 0.02\ s^{-1}\mu M^{-1}$, $K_B33(0) = 0.026\ s^{-1}\mu M^{-1}$ without EBIO. (C) Plot of apparent TBA exit rate ζPoK4 as a function of voltage measured either in the presence (filled squares) or in the absence (open squares) of EBIO. EBIO elicited an average 2.7-fold increase of the TBA exit rates. For voltages ranging from −150 to −30 mV, the apparent exit rate ζPoK4 decreased an e-fold factor per 90 mV for a voltage dependence with an electrical distance of 0.26 ± 0.02. The continuous lines represent the prediction of the model of Fig. 6 A computed according to Eq. 14 with $K_B41(0)$, $K_B42(0)$, and $K_B43(0)$ as in B. (D) Plot of the apparent TBA entry rate PoK3 as a function of voltage measured either in the presence (filled squares) or in the absence (open squares) of EBIO. Filled (EBIO) and open (no EBIO) diamonds show TBA entry rates K3 after correcting for the channel open probabilities Po. The resulting K3 values are shown to be comparable under both experimental conditions with a voltage dependence corresponding to an e-fold increase per 150 mV. The continuous lines represent the prediction of the model of Fig. 6 A, computed according to Eq. 13 with $K_B31(0)$, $K_B32(0)$, and $K_B33(0)$ as in B.

ternal medium and the TBA binding site cannot account for an electrical distance δ of 0.49 as observed experimentally (Fig. 5 B).

A minimal kinetic scheme describing the blocking action of TBA within the channel pore is shown in Fig. 6 A. A similar model has already been described by Heginbotham and Kutluay (2004). In many respects, this model incorporates some of the features of models previously proposed to account for the effect of external and internal permeant ions on the Kir1.1 and *Shaker* channels (Spassova and Lu, 1998, 1999; Thompson and Begenisich, 2003a,b). The model in Fig. 6 A includes the essential features of the single file diffusion process in the selectivity filter recently described for the KcsA channel for $K^+$ ion concentrations within the range of our experimental conditions ($K^+$ ion activity of 140 mM) (Berneche and Roux, 2003). In the unblocked mode, $K^+$ ion efflux is seen as a sequence of changes in the ion occupancy state of the pore with [S3,S1] ↔ [S5,S3,S1] ↔ [S4,S2,S0] ↔ [S4,S2] and back to [S3,S1]. The sites referred to as S0 and S5 are located outside the selectivity filter and correspond to the channel external $K^+$ binding site and central cavity, respectively. The model also considers the possibility of a $K^+$ ion in S5 with S4 occupied (states [S5,S4,S2] and [S5,S4,S2,S0]). An interaction factor termed "f" has in this case been introduced to account for the change in $K^+$ entry and exit rates ki and ke due to the presence of a $K^+$ ion in S4. The rates describing the transitions [S5,S3,S1] ↔ [S5,S4,S2] and [S3,S1] ↔ [S4,S2] become in this case related, so that $k3/k4 = f^2$ (k1/k2). Fig. 6 C presents the free energy profiles calculated for a $K^+$ ion along the pore axis for the [S4,S2] and [S3,S1] filter configurations. These calculations predict a maximum difference of 1.8 kcal/M between the [S5,S4,S2] and [S5,S3,S1] configurations, for an f factor corresponding approximately to 0.22.

Calculations were first performed to determine to what extent the model proposed in Fig. 6 A accounts

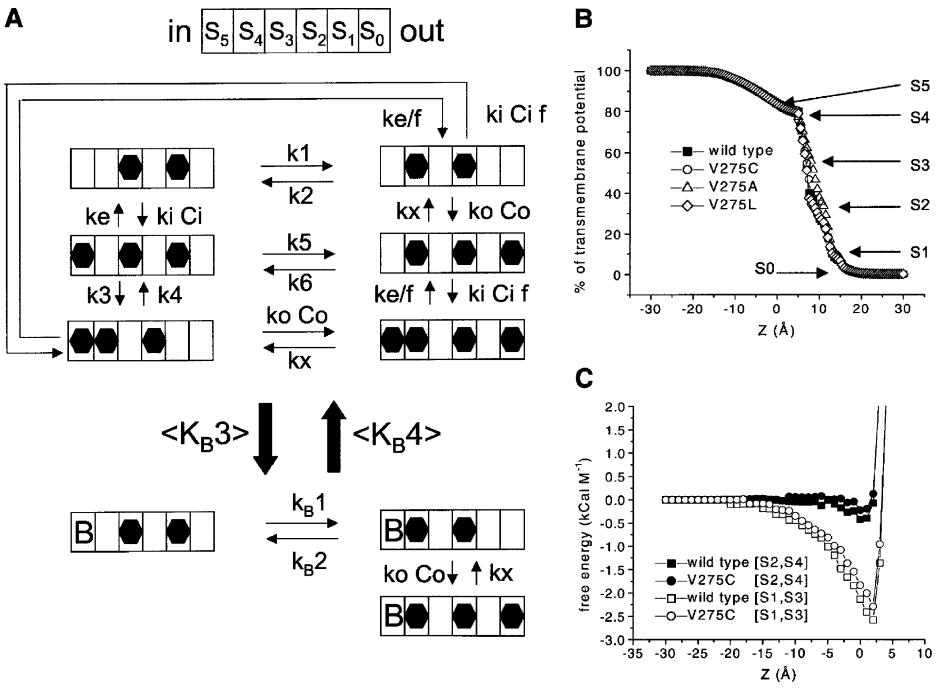


FIGURE 6. Proposed mechanism for the IKCa block by internal TBA. (A) The channel pore region is pictured as six distinct binding sites for $K^+$ ions, with S1 to S4 the binding sites for $K^+$ ions in the selectivity filter and S5 and S0 the channel central cavity and external $K^+$ ion binding site, respectively. In this model, TBA blocks the pore by entering the open channel from the cytoplasmic side up to the inner cavity (S5), where it binds without going through the selectivity filter. In the unblocked mode, $K^+$ ion (filled dot) flux is described as a sequence of changes in the ion occupancy configuration of the pore. $K^+$ ion efflux will be obtained following any of the paths starting with the entrance of an ion into S5 and leading to the hopping of an ion out of S0 to the external medium. Reversibly, any of the paths starting with an ion entering S0 and ending with the release on an ion from S5 into the inner medium will account for $K^+$ influx. A parameter f, with $f < 1$, is introduced to account for the effect of the occupancy state of S4 on the entry and exit rates of $K^+$ to and from the cavity (S5) so that ki and ke/f become higher than ki*f and ke, respectively. Formally, f corresponds to $\exp(-(E[S4,S2,z] - E[S3,S1,z])/2KT)$ where E[S4,S2,z] and E[S3,S1,z] correspond to the electrostatic energies of TBA along the pore axis for the [S4,S2] and [S3,S1] selectivity filter configurations, respectively. For $z = 0$, the energy profile in C predicts $f = 0.22$. Identical sequences for the occupation states are hypothesized for the pore in the blocked configuration. The mean entry and exit rates of TBA to/from S5 ($<K_B3>$ and $<K_B4>$) will strictly depend on the ion occupancy state of the rest of the pore (see Eqs. 13 and 14). The voltage dependence of the rate constants was derived from the potential profile presented in B so that $k1 = k1(0)\exp(-0.23Vq/KT)$, $k2 = k2(0)\exp(0.23Vq/KT)$, $k3 = k3(0)\exp(-0.23Vq/KT)$, $k4 = k4(0)\exp(0.23Vq/KT)$, $k5 = k5(0)\exp((\alpha/2 - 0.23)Vq/KT)$, $k6 = k6(0)\exp(-(\alpha/2 - 0.23)Vq/KT)$, $ki = ki(0)\exp(0.5\ (1 - \alpha)Vq/KT)$, $ke = ke(0)\exp(-0.5(1 - \alpha)Vq/KT)$, $k_B1 = k_B1(0)\exp(-0.23Vq/KT)$, and $k_B2 = k_B2(0)\exp(0.23Vq/KT)$, with $\alpha$ referring to the fraction of potential V applied between S5 (cavity region) and the external solution. The external binding site S0 and the external medium being equipotential (B), the rate constants ko and kx were considered voltage insensitive. It was assumed finally that the voltage dependence in each transition was partitioned evenly between forward and backward rates. (B) Transmembrane potential profile computed by solving the Poisson-Boltzmann equation for the pore region of the wild-type IKCa, V275C, V275A, and V275L channels. The IKCa 3D structure was obtained by homology modeling using the MthK channel coordinates as template. These calculations indicated that 81% of the applied voltage is restricted to the selectivity filter region. The difference in potential between the cavity and the cytoplasmic medium accounts for <16% of the transmembrane potential. (C) Free energy profile for transferring an ion from the bulk medium to a point z ($x = y = 0$) along the channel central axis, computed for the IKCa wild-type and V275C channels (identical results were obtained for the V275A and V275L mutants). Calculations were performed in conditions where the selectivity filter was either in the [S4,S2] or [S3,S1] configuration. The coordinate $z = 0$ corresponds to the expected position of the V275 residue. The model predicts a maximum difference in energy of 1.8 kcal $M^{-1}$ at $z = 0$ for both channels.

for the channel current/voltage characteristics. The continuous line in Fig. 4 C represents the prediction of the model. Best results were obtained assuming a $K^+$ binding affinity in S0 (kx/ko) and S5 (ke(0)/ki(0)) of 45 mM and 70 mM, respectively, with a ratio k1(0)/k2(0) of 0.3. The difference between the [S4,S2] ↔ [S3,S1] transition rates k1(0) and k2(0) accounts for most of the channel rectification, and may be related to the fast blocking action of divalent cations such as $Ca^{2+}$ at a site close to S4 (Soh and Park, 2002). In these calculations, the fraction of potential drop between the cavity and the external medium $\alpha$ was set to 0.84 as suggested by the potential profile presented in Fig. 6 B. Clearly the model in Fig. 6 A in which the voltage dependence of the rate constants is determined according to Fig. 6 B, satisfactory describes the channel current–voltage relationship (Fig. 4 C).

The blocking action of TBA was next modeled assuming that the blocking agent cannot enter S5 (channel cavity) when the site is already occupied by a $K^+$ ion ([S5,S3,S1], [S5,S4,S2], and [S5,S4,S2, S0]). Again, the presence of TBA in S5 is likely to affect the transition [B,S3,S1] ↔ [B,S4,S2] by shifting the equilibrium toward the [S3,S1] filter configuration. If the location of TBA binding site corresponds to S5, the transition [B,S3,S1] ↔ [B,S4,S2] should be such that $k_B1/k_B2 = k3/k4$. Strong interactions between TBA and the $K^+$ ions in the selectivity filter have already been postu-

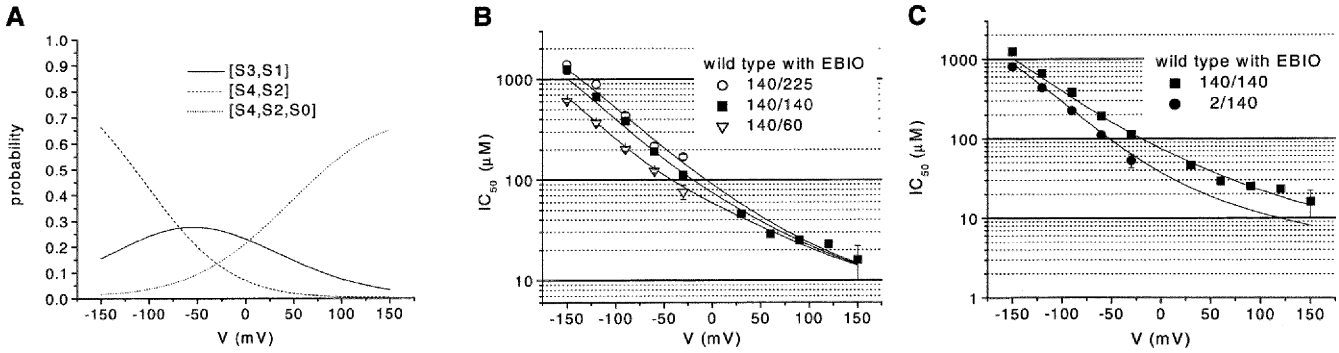


FIGURE 7. Effect of external and internal $K^+$ ion activity on TBA block. In A, the probabilities of the [S3,S1], [S4,S2], or [S4,S2,S0] channel states are plotted as a function of membrane voltage. At hyperpolarizing potentials, the [S4,S2] state is favored and its probability decreases monotonically with depolarization. In contrast, the probability of the [S4,S2,S0] state increases monotonically from close to zero at negative potentials to a maximum probability of 0.65 with depolarization. Finally, the probability of the [S3,S1] state showed little variations within the voltage range −100 to 0 mV. (B) Effect of changing the extracellular $K^+$ ion activity ($\alpha_{Ko}$) on the voltage dependence of IKCa block. Experiments were performed on IKCa wild-type channel with $\alpha_{Ko}$ = 60 mM (solution 50 $K_2SO_4$, open triangles), 140 mM (solution 200 $K_2SO_4$, filled squares), or 225 mM (solution 400 $K_2SO_4$, open circles) respectively, keeping the intracellular $K^+$ activity constant $\alpha_{Ki}$ at 140 mM (solution 200 $K_2SO_4$). Decreasing $\alpha_{Ko}$ resulted in a decrease in $IC_{50}$ over the entire voltage range. Also, increasing $\alpha_{Ko}$ led to an increase in the apparent electrical distance δ computed within the voltage range −150 to −30 mV, with δ values of 0.44 ± 0.01 ($n$ = 4), 0.49 ± 0.01 ($n$ = 4), and 0.52 ± 0.03 ($n$ = 4) for $\alpha_{Ko}$ = 60, 140, and 225 mM, respectively. Theoretical curves (continuous lines) were generated using the rate constant values given in Fig. 5 B. These results indicate that the occupancy of S5 depends on the external potassium activity, which is consistent with the model in Fig. 6 A. (C) Effect of $\alpha_{Ki}$ on the voltage dependence of IKCa block. Experiments were performed with $\alpha_{Ki}$ = 140 mM (solution 200 $K_2SO_4$, squares) or 2 mM (solution 1 $K_2SO_4$, circles), keeping $\alpha_{Ko}$ constant at 140 mM (solution 200 $K_2SO_4$). Decreasing $\alpha_{Ki}$ resulted in a decrease of $IC_{50}$ over the entire voltage range and led to an increase of the apparent electrical distance δ computed at negative potentials, with δ = 0.54 ± 0.01 ($n$ = 3) in 2 mM internal $K^+$ conditions and 0.49 ± 0.02 ($n$ = 6) in symmetrical 140 mM/140 mM $K^+$. These results are consistent with a competition between potassium and TBA for the site in S5, as proposed in Fig. 6 A. Theoretical curves (continuous lines) were generated using the rate constant values given in Fig. 5 B.

lated (French and Shoukimas, 1981) but never derived from structural considerations (Guo and Lu, 2001; Thompson and Begenisich, 2003b). In the model for TBA block proposed in Fig. 6 A, the entry rate of TBA is assumed to depend on the actual ion occupancy state of the pore with entry rates $K_B31 = K_B31(0)\exp(0.5(1-\beta)Vq/KT)$, $K_B32 = K_B32(0)\exp(0.5(1-\beta)Vq/KT)$, and $K_B33 = K_B33(0)\exp(0.5(1-\beta)Vq/KT)$, when the pore is in state [S4,S2], [S4,S2,S0], and [S3,S1], respectively (for example see MacKinnon and Miller, 1988; Thompson and Begenisich, 2003a). The parameter β refers to the fraction of the potential that is applied between the TBA binding site and the external medium. In conditions where the TBA binding site corresponds exactly to the channel central cavity, we have $\beta = \alpha \cong 0.84$ (Fig. 6 B). As the ion occupancy in these sites can be considered in equilibrium relative to the entry and exit rates of TBA, the average number of transitions between the unblocked and the blocked pore configuration can be expressed as

$$<K_B3> = e^{(0.5(1-\beta)Vq/KT)}[K_B31(0)P[S4,S2] + K_B32(0)P[S4,S2,S0] + K_B33(0)P[S3,S1]], \quad (13)$$

where P[S3,S1], P[S4,S2], and P[S4,S2,S0] are the probabilities for the unblocked channel selectivity filter to be in the [S3,S1], [S4,S2], or [S4,S2,S0] configurations, respectively. The variations in P[S3,S1], P[S4,S2], and P[S4,S2,S0] computed as a function of voltage are presented in Fig. 7 A. As seen, the probability of the [S4,S2] state is highly favored at negative potentials, whereas positive potentials increase the probability of the [S4,S2,S0] filter state. For potentials ranging from −100 to −30 mV, the probability of the state [S3,S1] appeared to vary within <15%. This analysis shows that the voltage dependence of the entry rate $<K_B3>$ predicted by Eq. 13, is expected to vary as a function of voltage in a complex manner.

In the blocked configuration, the exit rate of the blocking agent is assumed to depend similarly upon the ion occupancy state of the channel filter with exit rates $K_B41 = K_B41(0)\exp(-0.5(1-\beta)Vq/KT)$, $K_B42 = K_B42(0)\exp(-0.5(1-\beta)Vq/KT)$, and $K_B43 = K_B43(0)\exp(-0.5(1-\beta)Vq/KT)$ when the pore is in state [B,S4,S2], [B,S4,S2,S0], and [B,S3,S1], respectively. The average exit rate $<K_B4>$ then reads

$$<K_B4> = e^{(-0.5(1-\beta)Vq/KT)}[K_B41(0)P[B,S4,S2] + K_B42(0)P[B,S4,S2,S0] + K_B43(0)P[B,S3,S1]], \quad (14)$$

where P[B,S4,S2], P[B,S4,S2,S0], and P[B,S3,S1] are the probabilities for the filter to be in the [B,S4,S2], [B,S4,S2,S0], and [B,S3,S1] configuration for the blocked channel. In conditions where $K_B41(0) \cong$

$K_B42(0) = K_{out}$, the mean rate of transitions $<K_B4>$ reduces to

$$<K_B4> = \frac{K_{out}e^{(-0.5(1-\beta)Vq/KT)}}{(1+Kb)} + \frac{K_B43(0)e^{(-0.5(1-\beta)Vq/KT)}Kb}{(1+Kb)} \quad (15)$$

with

$$Kb = Ke\left(1+\frac{Co}{Ko}\right), \quad (16)$$

where Co is the external potassium ion concentration, $Ke = [k_B1(0)/k_B2(0)]\exp(-0.46\ Vq/KT)$ and $Ko = k_X/k_O$ the affinity of the external site (S0) for $K^+$. It is important to notice that if the blocker exit rate were assumed to be independent of the ion occupancy state of the filter ($K_B41(0) \cong K_B42(0) \cong K_B43(0) = K_{out}$), the voltage dependence of $<K_B4>$ would become $0.5(1-\beta)$ with $\beta = 0.84$. This would correspond to an e-fold change in $<K_B4>$ per 310 mV, which was never observed experimentally.

The continuous line in Fig. 5 C shows the predicted voltage dependence of the exit rate for the wild-type IKCa channel as computed from Eq. 14. Calculations were performed using the values of k3, k4, kx, and ko obtained by curve fitting the model to the channel I/V curve with in addition $k_B1 = k3$ and $k_B2 = k4$. Data points could be best accounted for with $K_B41(0)$, $K_B42(0)$, and $K_B43(0)$ equal to 2.9 $s^{-1}$, 10.4 $s^{-1}$, and 0.63 $s^{-1}$ in control conditions and 8 $s^{-1}$, 28 $s^{-1}$, and 1.7 $s^{-1}$ in the presence of EBIO, respectively. Clearly, the model presented in Fig. 6 A can account for the voltage dependence of the TBA exit rate. The continuous line in Fig. 5 B shows the predicted voltage dependence of $IC_{50}$ for voltages ranging from −150 to +150 mV. $IC_{50}$ values were computed as the ratio of $<K_B4>/<K_B3>$ with $K_B31(0)$, $K_B32(0)$, and $K_B33(0)$ as unique adjustable parameters. Best results were obtained with $K_B31(0)$, $K_B32(0)$, and $K_B33(0)$ equal to 0.022 $s^{-1}\mu M^{-1}$, 0.07 $s^{-1}\mu M^{-1}$, and 0.1 $s^{-1}\mu M^{-1}$ in the presence of EBIO and 0.006 $s^{-1}\mu M^{-1}$, 0.02 $s^{-1}\mu M^{-1}$, and 0.026 $s^{-1}\mu M^{-1}$ in control conditions, respectively. As seen, the model presented in Fig. 6 A successfully predicts a voltage dependence with $\delta = 0.49$ over the voltage range −150 to −30 mV, despite a potential profile where only 16% of the transmembrane potential is effectively applied between the channel cavity and the cytoplasmic medium. Globally these results indicate that the voltage dependence of the internal TBA block reflects for the most part an interaction of TBA with the $K^+$ ions in the selectivity filter with a limited contribution coming from the difference in potential between the internal medium and the TBA binding site.

*Effect of the External $K^+$ Concentration on IKCa Blockade by TBA*

One of the main features of the model presented in Fig. 6 A concerns the effect of the internal and external $K^+$ concentrations on the kinetics of the TBA block. Eq. 16 predicts for instance that the exit rate $<K_B4>$ should be a function of the external $K^+$ ion concentration (Co) with $<K_B4>$ increasing at higher Co values. Fig. 7 B shows the voltage dependence of the TBA blockade for external $K^+$ ion activities ranging from 60 to 225 mM. As seen, increasing Co resulted, as expected, in a voltage-dependent increase in $IC_{50}$. For instance, the $IC_{50}$ measured at −90 mV for a $K^+$ ion activity of 60 mM was estimated at 203 ± 9 μM ($n = 4$) as compared with 437 ± 26 μM ($n = 4$) in 225 mM external $K^+$ ion conditions. Increasing Co resulted also in a variation of the apparent electrical distance δ obtained by curve fitting the data points to $IC_{50} = IC_{50}(0)\exp(-\delta Vq/KT)$ for $-150\ mV < V < -30\ mV$. This analysis led to δ values of 0.44 ± 0.01 ($n = 4$), 0.49 ± 0.02 ($n = 6$), and 0.52 ± 0.03 ($n = 4$) for 60, 140, and 225 mM external $K^+$, respectively. These results indicated that the apparent voltage dependence of the TBA block not only depends on the structural parameters underlying the transmembrane potential profile but also on the parameters that control ion flux.

The predictions of the model described in Fig. 6 A are shown in Fig. 7 B as continuous lines. The proposed model is seen to successfully account for the voltage dependence of $IC_{50}$ over the $K^+$ activity range considered. Fig. 8 A presents a 3D plot of the expected variation in δ as a function of the external and internal $K^+$ activities. The electrical distance δ was computed by fitting the predictions of the model for a given set of internal and external $K^+$ activities to an equation of the form $IC_{50} = IC_{50}(0)\exp(-\delta Vq/KT)$ for $-150\ mV < V < -30\ mV$. This analysis revealed that increasing external $K^+$ activity up to 50 mM results in a systematic increase in δ independently of the internal $K^+$ activity. For external $K^+$ activities >50 mM, the predicted voltage dependence of the TBA block is exclusively a function of the internal $K^+$ level. For instance, with an internal $K^+$ ion activity of 140 mM, the electrical distance δ was estimated at 0.44, 0.47, and 0.46 in 60, 140, and 225 mM external $K^+$, respectively. This is well within the values measured experimentally, despite the fact that the results in Fig. 7 B point toward a stronger increase in δ at high external $K^+$ activities.

*Effect of the Internal $K^+$ Concentration on IKCa Blockade by TBA*

Fig. 7 C presents the effect of internal $K^+$ (Ci) on the IKCa blockade by TBA. Reducing Ci appeared to facilitate the blocking action of internal TBA, as expected

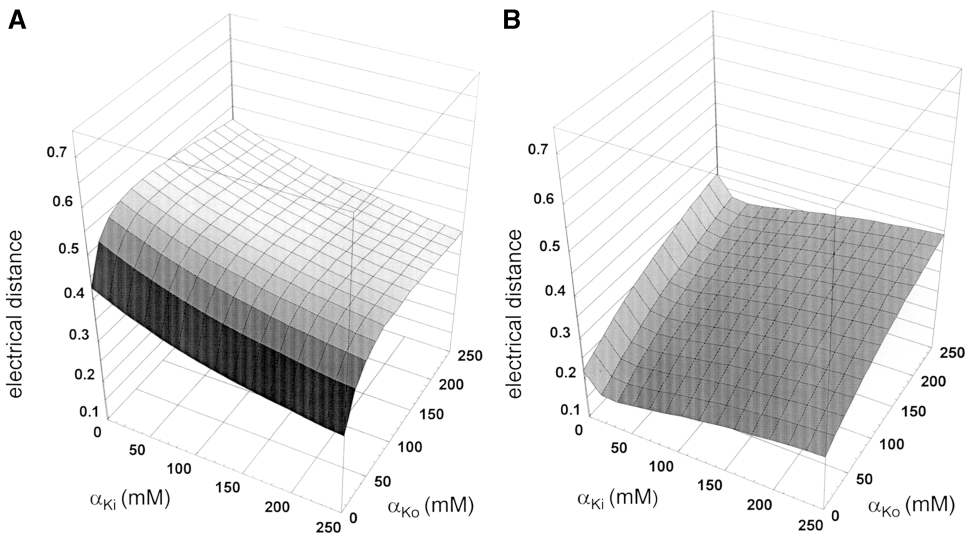


FIGURE 8. (A) 3D plot illustrating the effects of intracellular ($\alpha_{Ki}$) and extracellular ($\alpha_{Ko}$) $K^+$ ion activity on the apparent electrical distance δ, computed by curve fitting to a single exponential function the expected variations in $IC_{50}$ as a function of voltage predicted from the model in Fig. 6 A, for voltages ranging from −150 to −30 mV. As observed experimentally, increasing $\alpha_{Ki}$ at constant $\alpha_{Ko}$ causes a systematic reduction in δ. In 140 mM $\alpha_{Ko}$ for instance, the model predicts an apparent electrical distance δ of 0.56 for $\alpha_{Ki}$ = 2 mM, which is in accordance with the electrical distance observed experimentally. The model also predicts an increase in δ at increasing $\alpha_{Ko}$ for $\alpha_{Ko} < 50$ mM, with δ remaining close to 0.47 at higher $\alpha_{Ko}$ values. (B) 3D plot of the apparent electrical distance δ as a function of $\alpha_{Ko}$ and $\alpha_{Ki}$ computed over the voltage range 0–90 mV, with δ computed as described in A. Clearly the electrical distances δ computed at positive potentials (0–90 mV) are smaller than the values estimated at negative potentials under identical internal/external potassium conditions. These results point to an electrical distance for TBA block whose value depends on the potential range used to estimate the voltage dependence of the TBA block. Finally, increasing $\alpha_{Ki}$ is seen to result in an increase and not a decrease in δ value as shown in A.

for a system where the presence of a $K^+$ ion in S5 prevents the entry of TBA in the cavity. For instance, the TBA concentration for half inhibition at −30 mV decreased from 113 ± 5 μM ($n$ = 6) in 140 mM, to 53 ± 10 μM ($n$ = 3) in 2 mM internal $K^+$ conditions. The voltage dependence of the TBA block in low (2 mM) and high (140 mM) internal $K^+$ is also illustrated in Fig. 7 C. Clearly, the voltage sensitivity of the block over the voltage range −150 to −30 mV is increased by lowering internal concentration of $K^+$, with an electrical distance δ equal to 0.54 ± 0.01 ($n$ = 3) in 2 mM internal/140 mM external $K^+$ conditions, as compared with 0.49 ± 0.02 ($n$ = 6) in symmetrical 140 mM/140 mM $K^+$, respectively. The predictions of the model proposed in Fig. 6 A are represented as continuous lines (Fig. 7 C). The model was found to satisfactorily account for the variation in the voltage dependence of $IC_{50}$ as a function of Ci, and correctly predict that decreasing Ci should lead to a decrease in δ independently of Co (Fig. 8 A). In 140 mM external $K^+$ for instance, the model predicts an apparent electrical distance δ of 0.56 in 2 mM internal $K^+$, which is in accordance with the electrical distance observed experimentally.

*Effect of V275 Mutations on the Voltage Dependence of the TBA Block*

The results by Zhou et al. (2001) and the observations in Fig. 3 strongly suggest that the TBA interaction site is located in close proximity of the cavity lining residue V275. On this basis, we hypothesized that a shift of the TBA position relative to the selectivity filter, obtained by mutating V275, might affect the voltage dependence of the TBA block through an effect on the interactions between the blocking agent and the ions in the selectivity filter. Examples of reversible current block measured at increasing doses of TBA for the V275A, V275L, and V275C mutants are illustrated in Fig. 9 A. The resulting TBA–current inhibition dose–response curves measured at −60 mV in symmetrical 140 mM $K^+$ + 100 μM internal EBIO conditions are presented in Fig. 9 B. First of all, we observed that mutating the V275 residue had an effect on TBA affinity: the mutation V275C shifted the dose–response curve toward smaller concentrations from an $IC_{50}$ of 192 ± 7 μM ($n$ = 12) for wild type to 18 ± 2 μM ($n$ = 4) for the V275C channel. In contrast, the V275A and V275L substitutions caused an increase of the $IC_{50}$ value to 262 ± 29 μM ($n$ = 6) and 607 ± 54 μM ($n$ = 3), respectively. Notably, the substitution V275L was also found to decrease the channel conductance for inward currents by 50% with a unitary conductance of 21 ± 2 pS ($n$ = 2) for voltages negative to −50 mV (unpublished data). The voltage dependence of the TBA block for the V275C, V275A, and V275L mutant channels is illustrated in Fig. 9 C. For voltages ranging from −150 to −30 mV, estimations of the equivalent electrical distance δ led to 0.50 ± 0.03 ($n$ = 3), 0.72 ± 0.03 ($n$ = 2), and 0.7 ± 0.06 ($n$ = 3) for the V275L, V275C, and V275A mutants, respectively. Clearly, the extent of the changes in TBA binding affinity did not correlate with the changes in electrical distance.

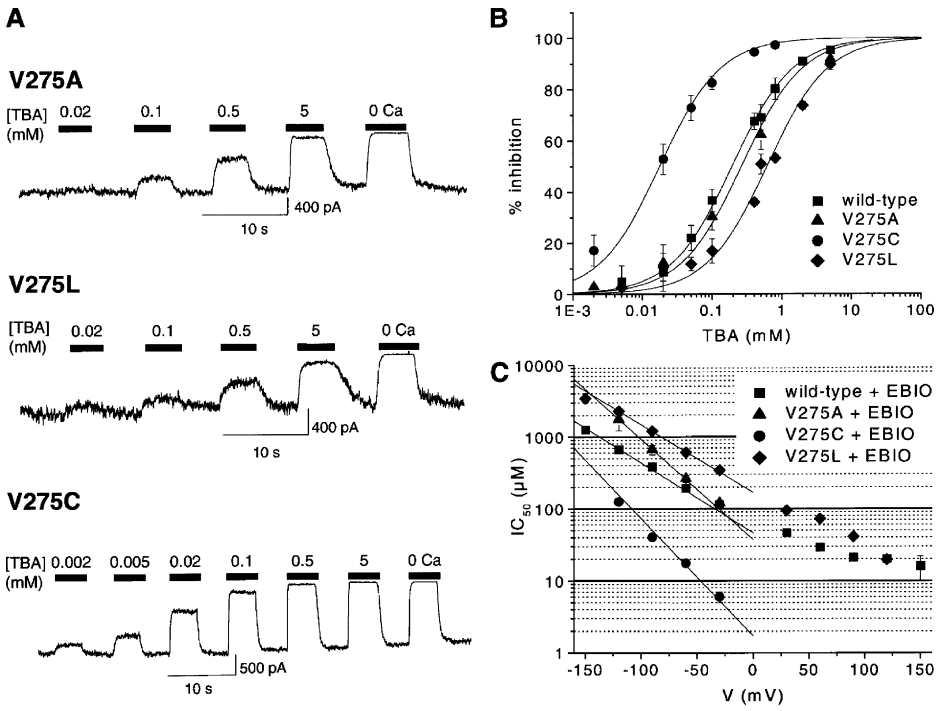


FIGURE 9. Effect of V275 mutations on the properties of the TBA-dependent block. (A) Inside-out current traces showing dose-dependent block of V275A, V275C, and V275L mutants by internal TBA. Experiments were performed in symmetrical 200 mM $K_2SO_4$ + 25 μM internal $Ca^{2+}$ and 100 μM EBIO conditions at a constant membrane potential of −60 mV. (B) TBA inhibition dose–response curves for the IKCa wild type and V275A, V275C, and V275L mutants. Data points were fitted to Eq. 1 and yielded $IC_{50}$ = 192 ± 7 μM for wild type ($n$ = 12), 262 ± 29 μM for V275A ($n$ = 5), 18.0 ± 1.7 μM for V275C ($n$ = 4), and 607 ± 54 μM for V275L ($n$ = 3). (C) Effect of mutating the V275 residue on the apparent electrical distance of the TBA blocking site δ measured in the voltage range between −150 and −30 mV. The TBA-dependent block $IC_{50}$ is plotted as a function of membrane voltage for wild-type IKCa and V275A, V275C, and V275L mutants. Mutations V275A and V275C led to δ = 0.7 compared with δ = 0.49 for the wild-type and V275L channels. These data indicate that the smaller residues engineered at position 275 are correlated to higher values of the apparent electrical distance of the TBA blocking site in the channel.

## DISCUSSION

In this study, we showed that the transmembrane potential profile computed from a model structure of the open IKCa channel derived from MthK is compatible with the voltage dependence of the channel block by internal TBA. Since the 3D structure of IKCa has not yet been solved, we cannot rule out the possibility that the open IKCa structure might differ from MthK. However, we showed in this work that a functional model that incorporates an interaction mechanism between TBA and the ions in the selectivity filter, together with transmembrane potential and free energy profiles derived from a MthK-like structure, can globally account for the complex behavior of IKCa block by TBA. In addition, evidence is presented that the voltage dependence of the TBA block can be modified by mutating the cavity lining V275 residue, suggesting that TBA position relative to the selectivity filter is important to the voltage dependence of the block. Finally, our data indicate that a model of TBA block derived from a MthK-like structure absolutely requires TBA to interact with the ions in the selectivity filter.

### *TBA Block in $K^+$ Selective Channels*

Quaternary alkylammonium ions have been used as probes to investigate the pore structure of a number of $K^+$ selective channels. It is generally agreed that the mechanism of channel block by ammonium ion from the cytoplasmic side involves an entry step into the open channel up to the channel central cavity where it binds without passing through the selectivity filter. The blocking action of QA ions is thus likely to reflect the internal structure of specific classes of $K^+$ channels. For instance, TBA was shown to block the inward rectifiers Kir2.1 and Kir1.1 at $IC_{50}(0)$ of 40 and 2 mM, respectively, with fractional electrical distances ≥1.0 arguing for an inner vestibule with single file diffusion properties (Guo and Lu, 2001). These values differ from the results reported in the present work with an $IC_{50}(0)$ of 70 μM and a fractional electrical distance at negative potentials δ of 0.49. Furthermore, the TBA entry rate for the Kir2.1 and Kir1.1 channels in zero current conditions (0 mV) was estimated at 0.004 $\mu M^{-1}s^{-1}$ compared with 0.07 $\mu M^{-1}s^{-1}$ in the present case. Clearly the inner pore region of IKCa seems to be less restrictive to TBA flow than that observed in Kir1.1 and Kir2.1. Fractional electrical distances ranging from 0.2 to 0.3 were reported for the voltage-gated *Shaker* and calcium-activated $K_{Ca}1.1$ channels, suggesting a weaker voltage dependence of the TBA block relative to IKCa (Villarroel et al., 1988; Choi et al., 1993; Ding and Horn, 2002; Thompson and Begenisich, 2003a; Li and Aldrich, 2004). However, the voltage sensitivity in both cases was measured at positive potentials in contrast to the protocols used in this work, where δ was estimated at negative potentials only. Fig. 8 B presents a 3D plot of the electrical distance δ computed from the model

in Fig. 6 A for positive voltages within 0 to +90 mV as a function of internal and external potassium activities. As seen, the electrical distance δ appeared significantly smaller when computed for positive than negative potentials over the entire external and internal potassium concentration range. For instance, the plot in Fig. 8 B shows that δ increases monotonically as a function of external potassium with a value of 0.24 in 150 mM internal/5 mM external $K^+$ and 0.32 in symmetrical 150 mM $K^+$ conditions. These values are well in agreement with the results obtained for *Shaker* and $K_{Ca}1.1$ and confirm that the apparent electrical distance associated with the TBA blocking mechanism is voltage variable. Furthermore, the results in Fig. 8 B indicate that increasing the internal potassium ion activity should lead to an increase in δ, as reported for the *Shaker* channel (Thompson and Begenisich, 2003a). The fact that the electrical distance varied as a function of the applied potential truly reflects a strong interaction between TBA and the ions in the selectivity filter. Finally, our results provide evidence for a regulation of the TBA block by internal and external $K^+$. In contrast to *Shaker*, competition by internal $K^+$ was apparent even in the absence of an external blocking agent such as TEA, suggesting a higher ion occupancy of S5 in IKCa compared with *Shaker* (Thompson and Begenisich, 2003a).

*TBA Block and IKCa Gating*

The present work also provides evidence for a reduction of the TBA $IC_{50}(0)$ by EBIO. EBIO has been documented to modulate SK and IKCa channels by stabilizing the interactions between $Ca^{2+}$-calmodulin and the channel α subunit (Pedarzani et al., 2001; von Hahn et al., 2001). An EBIO-dependent increase in Po could be detected by noise analysis at 25 μM internal $Ca^{2+}$ but not in nominally $Ca^{2+}$-free conditions (unpublished data). Our results would thus support a model whereby EBIO can activate IKCa at saturating $Ca^{2+}$ concentrations, in contrast to other reports (Pedersen et al., 1999; Syme et al., 2000; Pedarzani et al., 2001). The observation that EBIO led to a decrease in $IC_{50}(0)$ indicates that the IKCa opener affected Po and $Po^B$ differently, with the ratio ζ ($Po^B$/Po) becoming smaller after EBIO stimulation (see Eq. 2). One possible explanation would consist in $Po^B$ being higher than Po in the absence of EBIO, so that $Po^B$ would be relatively less affected by EBIO than Po. In support of this proposal is the observation of a 2.7-fold increase in $Po^B$ for a 3.8-fold increase in PoK3 in EBIO conditions (Fig. 5 C). Notably, the measured 3.8-fold increase in PoK3 elicited by EBIO fully correlates the Po increase estimated by noise analysis. These observations suggest therefore that the presence of TBA in the channel cavity affects the channel kinetic parameters as to either destabilize the channel closed configuration or stabilize the channel open state, or both. These results would be consistent with a model whereby TBA is trapped in the channel central cavity upon channel closing. Such a behavior would support a gating model where the TM6 helix bundle crossing in the closed configuration is small enough to constrict TBA flow from the channel central cavity to the internal medium. We cannot however rule out the possibility that the state dependency of the TBA block might result from a variation upon channel closing in the interactions between TBA and the pore residues involved in TBA binding. Such a mechanism would lead to a state-dependent kinetics of TBA block, without a trapping mechanism involving the TM6 bundle crossing (Li and Aldrich, 2004).

*Mutations of V275 and Voltage Dependence*

The present work shows that the voltage dependence of the TBA block is modified by mutating the cavity lining residue V275. Our results indicate for instance that the fractional distance δ measured over the voltage range −150 to −30 mV is increased from 0.49 to 0.70 by substituting the Val at 275 by either a Cys or an Ala, whereas the mutation V275L left δ unchanged. Mutating the V275 residue was also found to affect the binding affinity of the TBA receptor, but this effect appeared uncorrelated with the associated changes in δ. For instance, both V275C and V275A led to a δ value of 0.7 despite an $IC_{50}(0)$ for the V275C mutant 20 times smaller than for V275A. Similarly, the V275L mutation caused a threefold increase in $IC_{50}(0)$ relative to wild type without a significant change in δ. We cannot rule out, however, that part of the observed effects on $IC_{50}(0)$ may be related to a modification of the channel open probability, as indicated by our EBIO results. These observations differ somehow from the results obtained on *Shaker*, where changing the affinity of the external TEA receptor was reported to affect the voltage dependence of the TEA block (Heginbotham and MacKinnon, 1992). It was concluded in this case that the substitution Y499T moved the TEA binding site further into the pore.

The electrostatic free energy profiles presented in Fig. 6 C, predict that the magnitude of the interactions between TBA and the ions in the selectivity filter should be highly sensitive to the position of TBA within the channel cavity ($-3$ Å $< z <$ 3 Å). In contrast, the results in Fig. 6 B show that a shift in TBA position over the same distance range should minimally affect the potential difference between the TBA binding site and the internal medium ($[1 - \beta]$). Fig. 10 presents the expected variation in electrical distance for TBA block at negative potentials calculated on the basis of the transmembrane potential and energy profiles illustrated in Fig. 6 (B and C). As seen, the electrical distance δ increased from 0.30 to 0.62 for z varying from −3 to 3 Å . In contrast, $1 - \beta$ changed from 0.12 to 0.18 over the same

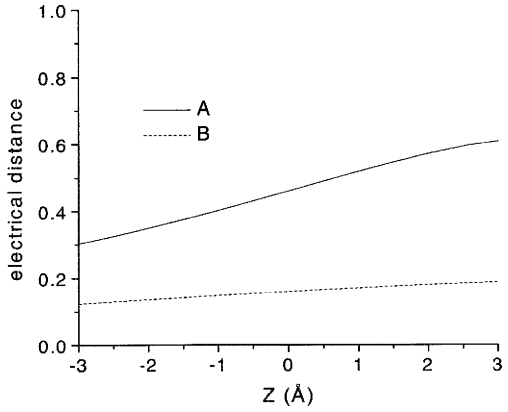


FIGURE 10. (A) Expected variation of the electrical distance for TBA block at negative potentials. Calculations based on the transmembrane and electrostatic energy profiles illustrated in Fig. 6 (B and C). The equilibrium constant $k_B1(0)/k_B2(0)$ was computed as $(k1(0)/k2(0))f^2$, with $f^2 = \exp(-(E[S4,S2,z] - E[S3,S1,z])/KT)$, where E[S4,S2,z] and E[S3,S1,z] correspond to the electrostatic energies of a charged particle along the pore axis for the [S4,S2] and [S3,S1] selectivity filter configurations, respectively. The effect of the electrostatic interactions on the TBA entry and exit rates was taken into account using $K_B43(0)/K_B41(0) = f$; $K_B42(0)/K_B41(0) = K_B40f$; $K_B31(0)/K_B33(0) = f$, and $K_B32(0)/K_B33(0) = K_B30f$, with $K_B30$ and $K_B40$ estimated from the curve fitting parameters obtained for TBA block assuming TBA located at $z = 0$ ($\alpha = 0.84$). (B) Expected electrical distance between the TBA binding site and the internal medium. $(1 - \beta)$.

distance range. Clearly the proposed model for TBA block predicts an increase in δ measured at negative potentials that far exceeds the associated change in electrical distance $1 - \beta$. The fact that the V275C and V275A mutations resulted in a TBA block with a stronger voltage dependence suggests, therefore, that the substitution of the Val at 275 (volume 140 Å$^3$) by residues of smaller sizes (108 Å$^3$ for Cys and 88 Å$^3$ for Ala) enabled TBA to penetrate further into the pore, closer to the selectivity filter. It is possible that the substitutions V275C and V275A allowed TBA to move closer to the T250 residue located at the entrance of the channel selectivity filter. Notably, the crystal structure reported by Zhou et al. (2001) predicts that T250 and V275 should be close to TBA, potentially contributing to the formation of the TBA binding site. Mutating the Val at 275 to a larger residue such as Leu (166 Å$^3$) did not seem to modify the position of the TBA relative to the selectivity filter, as the electrical distance δ remained unchanged. Our model could not, however, account for electrical distances >0.65, the electrostatic energy profiles illustrated in Fig. 6 C becoming less accurate for large interaction energies ($z > 3$ Å). Furthermore, we cannot rule out additional effects on the pore structure due to mutations at position 275 as the V275 residue is adjacent to the alleged TM6 gating hinge at G274. Finally, the observation that the V275L mutant showed a 50% smaller unitary conductance further demonstrated the importance of the 275 residue to the formation of the central cavity. In fact, the model in Fig. 6 A indicates that the 50% decrease in conductance with the V275L mutant can be ascribed to a decrease in the equilibrium constant k5(0)/k6(0), which accounts for the transitions of a $K^+$ ion between S4 and the channel cavity. Globally, these results support the model proposed in Fig. 6 A, where most of the voltage dependence of the TBA block is due to the blocking agent sensing the ion occupancy state of the selectivity filter.

*Conclusion*

The data presented in this work show that the electrical distance δ, which describes the voltage dependence of blocking agents such as TBA, is voltage variable and does not simply reflect the actual difference in potential between the blocker binding site and the internal medium. Our results rather support a model where the voltage dependence of charged blockers is controlled to a large extent by the ion occupancy state of the selectivity filter.

We thank Dr. Benoit Roux for stimulating discussions and for providing a copy of the manuscript on the intracellular TEA block of the KcsA potassium channel prior to publication. We also acknowledge the work of Ms. Julie Verner for expert oocyte preparation.

This work was supported by grants from the Canadian Institutes of Health Research (MOP 7769), from the Canadian Heart and Stroke Foundation, and from the Canadian Cystic Fibrosis Foundation.

Olaf S. Andersen served as editor.

*Submitted: 8 July 2004*
*Accepted: 1 September 2004*

REFERENCES

Berneche, S., and B. Roux. 2003. A microscopic view of ion conduction through the $K^+$ channel. *Proc. Natl. Acad. Sci. USA.* 100: 8644–8648.

Choi, K.L., C. Mossman, J. Aube, and G. Yellen. 1993. The internal quaternary ammonium receptor site of Shaker potassium channels. *Neuron.* 10:533–541.

Ding, S., and R. Horn. 2002. Tail end of the s6 segment: role in permeation in shaker potassium channels. *J. Gen. Physiol.* 120:87–97.

Doyle, D.A., J.M. Cabral, R.A. Pfuetzner, A. Kuo, J.M. Gulbis, S.L. Cohen, B.T. Chait, and R. MacKinnon. 1998. The structure of the potassium channel: molecular basis of $K^+$ conduction and selectivity. *Science.* 280:69–77.

French, R.J., and J.J. Shoukimas. 1981. Blockage of squid axon potassium conductance by internal tetra-N-alkylammonium ions of various sizes. *Biophys. J.* 34:271–291.

Garneau, L., H. Klein, L. Parent, and R. Sauve. 2003. Contribution of cytosolic cysteine residues to the gating properties of the kir2.1 inward rectifier. *Biophys. J.* 84:3717–3729.

Guo, D., and Z. Lu. 2001. Kinetics of inward-rectifier $K^+$ channel block by quaternary alkylammonium ions. Dimension and properties of the inner pore. *J. Gen. Physiol.* 117:395–406.

Heginbotham, L., and E. Kutluay. 2004. Revisiting voltage-dependent relief of block in ion channels: a mechanism independent of punchthrough. *Biophys. J.* 86:3663–3670.

Heginbotham, L., and R. MacKinnon. 1992. The aromatic binding site for tetraethylammonium ion on potassium channels. *Neuron.* 8:483–491.

Holmgren, M., P.L. Smith, and G. Yellen. 1997. Trapping of organic blockers by closing of voltage-dependent $K^+$ channels: evidence for a trap door mechanism of activation gating. *J. Gen. Physiol.* 109:527–535.

Ishii, T.M., C. Silvia, B. Hirschberg, C.T. Bond, and J.P. Adelman. 1997. A human intermediate conductance calcium-activated potassium channel. *Proc. Natl. Acad. Sci. USA.* 94:11651–11656.

Jiang, Y., A. Lee, J. Chen, M. Cadene, B.T. Chait, and R. MacKinnon. 2002a. Crystal structure and mechanism of a calcium-gated potassium channel. *Nature.* 417:515–522.

Jiang, Y., A. Lee, J. Chen, M. Cadene, B.T. Chait, and R. MacKinnon. 2002b. The open pore conformation of potassium channels. *Nature.* 417:523–526.

Joiner, W.J., L.-Y. Wang, M.D. Tang, and L.K. Kaczmarek. 1997. hSK4, a member of a novel subfamily of calcium-activated potassium channel. *Proc. Natl. Acad. Sci. USA.* 94:11013–11018.

Khanna, R., M.C. Chang, W.J. Joiner, L.K. Kaczmarek, and L.C. Schlichter. 1999. hSK4/hIK1, a calmodulin-binding KCa channel in human T lymphocytes. Roles in proliferation and volume regulation. *J. Biol. Chem.* 274:14838–14849.

Kohler, M., B. Hirschberg, C.T. Bond, J.M. Kinzie, N.V. Marrion, J. Maylie, and J.P. Adelman. 1996. Small-conductance, calcium-activated potassium channels from mammalian brain. *Science.* 273: 1709–1714.

Li, W., and R. W. Aldrich. 2004. Unique inner pore properties of BK channels revealed by quaternary ammonium block. *J. Gen. Physiol.* 124:43–57.

Logsdon, N.J., J. Kang, J.A. Togo, E.P. Christian, and J. Aiyar. 1997. A novel gene, hKCa4, encodes the calcium-activated potassium channel in human T lymphocytes. *J. Biol. Chem.* 272:32723–32726.

MacKinnon, R., and C. Miller. 1988. Mechanism of charybdotoxin block of the high-conductance, $Ca^{2+}$-activated $K^+$ channel. *J. Gen. Physiol.* 91:335–349.

Morier, N., and R. Sauvé. 1994. Analysis of a novel double-barreled anion channel from rat liver rough endoplasmic reticulum. *Biophys. J.* 67:590–602.

Pedarzani, P., J. Mosbacher, A. Rivard, L.A. Cingolani, D. Oliver, M. Stocker, J.P. Adelman, and B. Fakler. 2001. Control of electrical activity in central neurons by modulating the gating of small conductance $Ca^{2+}$-activated $K^+$ channels. *J. Biol. Chem.* 276:9762–9769.

Pedersen, K.A., R.L. Schroder, B. Skaaning-Jensen, D. Strobaek, S.P. Olesen, and P. Christophersen. 1999. Activation of the human intermediate-conductance $Ca^{2+}$-activated $K^+$ channel by 1-ethyl-2-benzimidazolinone is strongly $Ca^{2+}$-dependent. *Biochim. Biophys. Acta.* 1420:231–240.

Qin, F., A. Auerbach, and F. Sachs. 1996. Estimating single-channel kinetic parameters from idealized patch-clamp data containing missed events. *Biophys. J.* 70:264–280.

Qin, F., A. Auerbach, and F. Sachs. 1997. Maximum likelihood estimation of aggregated Markov processes. *Proc. R. Soc. Lond. B. Biol. Sci.* 264:375–383.

Rauer, H., M.D. Lanigan, M.W. Pennington, J. Aiyar, S. Ghanshani, M.D. Cahalan, R.S. Norton, and K.G. Chandy. 2000. Structure-guided transformation of charybdotoxin yields an analog that selectively targets $Ca^{2+}$-activated over voltage-gated $K^+$ channels. *J. Biol. Chem.* 275:1201–1208.

Rittenhouse, A.R., D.H. Vandorpe, C. Brugnara, and S.L. Alper. 1997. The antifungal imidazole clotrimazole and its major in vivo metabolite are potent blockers of the calcium-activated channel in murine erythroleukemia cells. *J. Membr. Biol.* 157:177–191.

Robinson, R.A., and R.H. Stokes. 1959. Electrolyte Solutions. 2nd ed. Butterworths, London. 571 pp.

Roux, B. 1997. Influence of the membrane potential on the free energy of an intrinsic protein. *Biophys. J.* 73:2980–2989.

Sali, A., and T.L. Blundell. 1993. Comparative protein modelling by satisfaction of spatial restraints. *J. Mol. Biol.* 234:779–815.

Schumacher, M.A., A.F. Rivard, H.P. Bachinger, and J.P. Adelman. 2001. Structure of the gating domain of a $Ca^{2+}$-activated $K^+$ channel complexed with $Ca^{2+}$/calmodulin. *Nature.* 410:1120–1124.

Simoes, M., L. Garneau, H. Klein, U. Banderali, F. Hobeila, B. Roux, L. Parent, and R. Sauve. 2002. Cysteine mutagenesis and computer modeling of the S6 region of an intermediate conductance IKCa channel. *J. Gen. Physiol.* 120:99–116.

Soh, H., and C.S. Park. 2002. Localization of divalent cation-binding site in the pore of a small conductance $Ca^{2+}$-activated $K^+$ channel and its role in determining current-voltage relationship. *Biophys. J.* 83:2528–2538.

Spassova, M., and Z. Lu. 1998. Coupled ion movement underlies rectification in an inward-rectifier $K^+$ channel. *J. Gen. Physiol.* 112:211–221.

Spassova, M., and Z. Lu. 1999. Tuning the voltage dependence of tetraethylammonium block with permeant ions in an inward-rectifier $K^+$ channel. *J. Gen. Physiol.* 114:415–426.

Syme, C.A., A.C. Gerlach, A.K. Singh, and D.C. Devor. 2000. Pharmacological activation of cloned intermediate- and small-conductance $Ca^{2+}$-activated $K^+$ channels. *Am. J. Physiol. Cell Physiol.* 278:C570–C581.

Thompson, J., and T. Begenisich. 2003a. Functional identification of ion binding sites at the internal end of the pore in Shaker $K^+$ channels. *J. Physiol.* 549:107–120.

Thompson, J., and T. Begenisich. 2003b. External TEA block of shaker $K^+$ channels is coupled to the movement of $K^+$ ions within the selectivity filter. *J. Gen. Physiol.* 122:239–246.

Vandorpe, D.H., B.E. Shmukler, L. Jiang, B. Lim, J. Maylie, J.P. Adelman, L. de Franceschi, M.D. Cappellini, C. Brugnara, and S.L. Alper. 1998. cDNA cloning and functional characterization of the mouse $Ca^{2+}$-gated $K^+$ channel, mIK1. Roles in regulatory volume decrease and erythroid differentiation. *J. Biol. Chem.* 273: 21542–21553.

Vergara, C., R. Latorre, N.V. Marrion, and J.P. Adelman. 1998. Calcium-activated potassium channel. *Curr. Opin. Neurobiol.* 8:321–329.

Villarroel, A., O. Alvarez, A. Oberhauser, and R. Latorre. 1988. Probing a $Ca^{2+}$-activated $K^+$ channel with quaternary ammonium ions. *Pflugers Arch.* 413:118–126.

von Hahn, T., I. Thiele, L. Zingaro, K. Hamm, M. Garcia-Alzamora, M. Kottgen, M. Bleich, and R. Warth. 2001. Characterisation of the rat SK4/IK1 $K^+$ channel. *Cell. Physiol. Biochem.* 11:219–230.

Warth, R., K. Hamm, M. Bleich, K. Kunzelmann, T. von Hahn, R. Schreiber, E. Ullrich, M. Mengel, N. Trautmann, P. Kindle, et al. 1999. Molecular and functional characterization of the small $Ca^{2+}$-regulated $K^+$ channel (rSK4) of colonic crypts. *Pflugers Arch.* 438:437–444.

Warwicker, J., and H.C. Watson. 1982. Calculation of the electric potential in the active site cleft due to alpha-helix dipoles. *J. Mol. Biol.* 157:671–679.

Woodhull, A.M. 1973. Ionic blockage of sodium channels in nerve. *J. Gen. Physiol.* 61:687–708.

Wulff, H., G.A. Gutman, M.D. Cahalan, and K.G. Chandy. 2001. Delineation of the clotrimazole/TRAM-34 binding site on the intermediate conductance calcium-activated potassium channel, IKCa1. *J. Biol. Chem.* 276:32040–32045.

Zhou, M., J.H. Morais-Cabral, S. Mann, and R. MacKinnon. 2001. Potassium channel receptor site for the inactivation gate and quaternary amine inhibitors. *Nature.* 411:657–661.